Glass-to-Crystal Transition in the NASICON Glass-Ceramic System $Na_{1+x}Al_xM_{2-x}(PO_4)_3$ (M = Ge, Ti)

Henrik Bradtmüller,[1] Adriana M. Nieto-Munoz,[2] Jairo F. Ortiz-Mosquera,[2] Ana Candida Martins Rodrigues,[2] and Hellmut Eckert,[1,3*]

[1]*Institut für Physikalische Chemie, WWU Münster, Corrensstraße 30, D48149 Münster, Germany*

[2]*Departamento de Engenharia de Materiais, Universidade Federal de São Carlos, CP 676, 13565-905, São Carlos, SP, Brasil.*

[3]*Instituto de Física de São Carlos, Universidade de São Paulo, CP 369. São Carlos, SP 13566-590, SP. Brazil*

Abstract

The glass-to-crystal transition of $Na_{1+x}Al_xGe_{2-x}(PO_4)_3$ (NAGP), and $Na_{1+x}Al_xTi_{2-x}(PO_4)_3$ (NATP), both crystallizing in variants of the Na-superionic conducting (NASICON) structure, has been investigated by solid-state NMR. The ceramic materials produced by annealing the precursor glasses above the glass transition temperature are candidate materials for solid-state separator membranes in sodium ion batteries. The different local structural environments involving both network former and network modifier species have been characterized by comprehensive ^{23}Na, ^{27}Al and ^{31}P magic angle spinning nuclear magnetic resonance (MAS NMR) experiments. In crystalline $Na_{1+x}Al_xGe_{2-x}(PO_4)_3$ samples multiple phosphate environments are observed, corresponding to *n* Al and 4-*n* Ge species in their second coordination spheres. In contrast, no site resolution is observed in the analogous $Na_{1+x}Al_xTi_{2-x}(PO_4)_3$ (NATP) system. This can be understood on the basis of X-ray powder diffraction (XRD) data, which reveal a significant lattice expansion in the former, but no lattice expansion in the latter material. ^{27}Al MAS-NMR data reveal that in the glassy state, Al occurs with coordination numbers four, five and six, with the fraction of four-coordinated Al being substantially higher in the NATP glasses than in the NAGP glasses. ^{23}Na MAS-NMR and spin echo decay measurements reveal distinct differences between glassy and crystallized materials with regard to the local environments and the spatial distributions of the sodium ions.

Key words: *NASICON, glass ceramic, nuclear magnetic resonance.*

Introduction

Much effort in recent materials science has been focused on the development of energy storage devices which simultaneously possess high-energy and high-power properties [1,2]. From the viewpoint of cycling stability and operating safety all-solid-state batteries featuring fast-ion conducting electrolytes are preferred over lithium-ion batteries with liquid electrolytes [3-5]. The principal challenge lies with the creation of materials with sufficiently high ionic conductivity and general stability at atmospheric- and electrochemical conditions. Promising crystalline materials include solid electrolytes crystallizing in the Na-superionic conductor (NASICON) structure [6]. This versatile structure, featured by the general compositional formula $A(I)_{1+2w+x-y+z}M(II)_wM(III)_xM(V)_yM(IV)_{2-w-x-y}(SiO_4)_z(PO_4)_{3-z}$ gives rise to a large family of highly conducting solid electrolytes. Here we consider crystalline solid solutions based on a fundamental composition $A(I)M(IV)_2(PO_4)_3$ in which the tetravalent ion M(IV) is substituted by trivalent ions. Charge balance is restored by incorporation of a corresponding amount of monovalent A cations (usually Li, Na or Ag), which are accommodated on interstitial sites in the structure [8]. Homogeneity regions depend on cation radius ratios and also turn out to be strongly influenced by preparation and processing conditions. While materials have been traditionally prepared via solid-state reactions ("sintering route"), preparations involving the crystallization of precursor glasses ("glass-ceramic route") have resulted in more homogeneous materials with controllable microstructures and morphologies. The NASICON structure features two distinct sites for the monovalent species, called M1 and M2, which are present in a ratio of 1:3. The preferred ionic pathway is assumed to involve a sequence of M1->M2->M1 jumps through interstitial windows [9]. As the latter present the kinetic bottleneck of ionic motion, recent studies have attempted to modify window sizes, by substituting the M(IV) ion either by isovalently or aliovalently by a trivalent ion such as Al^{3+} or Cr^{3+} [10-18].

While the majority of work on NASICON publications focuses on lithium-containing systems, the parallel exploration of sodium-bearing materials is motivated by the (compared to lithium) 500-fold atomic abundance of the element sodium in the earth's crust and its much more widespread geographical distribution. Thus, large-scale efforts will be sustainable and attractive to national energy economies. In the present contribution, we discuss glasses and glass-ceramics of composition $Na_{1+x}Al_xGe_{2-x}(PO_4)_3$ (NAGP) and $Na_{1+x}Al_xTi_{2-x}(PO_4)_3$ (NATP) ($0.4 \leq x \leq 1.0$) together with NGP, the aluminum free composition ($x = 0$). This study

extends previous studies reporting electrical conductivities and standard solid state characterization of exclusively crystalline members of the NAGP [19,20] and NATP [21] families in the compositional regimes of $0.3 \leq x \leq 1.0$ and $0 \leq x \leq 0.9$ respectively, and allows a comparison with respect to the related lithium NASICON materials [11,22]. In particular, we will make extensive use of solid-state nuclear magnetic resonance (NMR) spectroscopy, to characterize the glass-to-crystal transition in the NAGP and NATP systems. While NMR has already been widely applied for the study of lithium-containing NASICON materials [11,23-29] results on crystalline sodium-containing NASICON powders are scarce [30,31] and to date, no experimental characterization of the precursor glasses and of glass-ceramic materials has been done.

Key words: *solid state NMR, NASICON, glass ceramic, glass-to-crystal transition*

Experimental Section

Sample Preparation and Characterization

Vitreous $Na_{1+x}Al_xM_{2-x}(PO_4)_3$ (M = Ge, Ti) samples were prepared in 20 gram batches by the standard melt-quench process and subsequent heat treatment. Finely ground Na_2CO_3 (Vetec, 99.5%), Al_2O_3 (Aldrich 99%) GeO_2 (Aldrich 99%), TiO_2 (Aldrich 99.9%) and $NH_4H_2PO_4$ (Aldrich 98%) were mixed in the ratios corresponding to the desired sample compositions (listed in Table 1) and heated in a platinum crucible in three steps: (1) heating from room temperature to 673 K at 10 K/min with a holding time of 4 h at 673 K (2) heating to 973 K at 10 K/min , and holding time of 2 h at 973 K to ensure the complete removal of CO_2, NH_3 and H_2O, (3) melting for 30 min at 1573–1653 K, and 1723 K for NAGP and NATP glass respectively. To ensure homogenization, glasses were splat-cooled after 30 min, then re-melted at same temperature for more 30 min. After rapid splat cooling, small brittle glass pieces of 1.5 mm thickness and areas ranging from 10 – 100 mm^2 were obtained. NAGP glasses were transparent and colorless, while NATP glasses were violet-colored and contained, depending on the aluminum content, spots of crystalline phase, reflecting the great tendency of these glasses to crystallize. This purple color was already found in the lithium homologue, LATP glass and was attributed to the presence of Ti^{3+} ions, reduced from Ti^{4+} during the melting procedure [12]. Glass transition (T_g) and crystallization temperatures (T_x) were measured by differential scanning calorimetry (DSC) on a DSC 404 NETZSCH system (heating rate 10 K min^{-1}).

Glass-ceramics were obtained by a heat treatment of the precursor glasses at each composition's crystallization temperature (temperature T_x, measured at the onset of the crystallization peak, for 3 hrs and 30 min, for NAGP and NATP. T_x varied with the increase in Al content, from 919 to 939 K for NAGP and from 940 to 992 K for NATP . In the case of crystallization heat treatment, samples were inserted directly in a pre-heated oven at T_x The crystalline phases of the glass-ceramics were characterized by X-ray diffraction (XRD) on a Rigaku Ultima IV diffractometer, operating with Cu K_α radiation generated at 20 mA and 40 kV and integration times of 0.6 s at 0.02° steps. Diffraction peak indexing and lattice constant analysis was done using the QualX [32] and Expo2014 [33] software by Altomare et al., in combination with the Crystallography Open Database (COD) [34]. Densities were obtained by Archimedes' principle using an analytical balance and water as fluid media.

Solid State NMR

NMR spectra were obtained at 11.7 T (Bruker DSX-500), 9.4 T (Bruker DSX-400), 5.7 T (Varian 240-MR DD2) and 4.7 T (Bruker DSX-500) with commercially available 4 mm triple resonance MAS probes and MAS spinning rates varying from 10.0 to 15.0 kHz. The data were analyzed with the DMFIT software package [35]. ^{31}P MAS NMR spectra were measured at 98.12 MHz with $\pi/2$-pulse durations of 4 μs length and recycle delays of 1200 to 1400 s. Chemical shifts are reported relative to BPO_4 (measured at -29.3 ppm relative to 85% H_3PO_4). The spectra were deconvoluted into Gaussian components. ^{27}Al MAS NMR spectra were measured at 63.16 MHz using pulses with small flip angles (30°) of 1.3 μs duration and recycle delays of 0.5 to 1 s. Chemical shifts are reported relative to AlF_3 (measured at −16.05 ppm relative to a 1M aqueous solution of $Al(NO_3)_3$).

^{23}Na MAS NMR spectra were measured at 64.12 MHz using small flip angle pulses (30°) of 0.7 μs duration and recycle delays varying between 0.25 and 5 s. The chemical shifts are reported using solid NaCl (7.2 ppm vs 1 M aqueous NaCl solution [36]) as a secondary reference. The central transition spectra of these quadrupolar nuclei were fitted according to the Czjzek model [37]. ^{23}Na Triple Quantum Magic Angle Spinning (TQMAS) spectra were recorded at carrier frequencies of the standard MAS NMR experiments using a three-pulse sequence with z-filter [38]. The employed pulse lengths were close to 4.8 and 1.8 μs at a nutation frequency of 114 kHz for the first two hard pulses. The duration of the soft third pulse was 9.5 to 11.0 μs at a nutation frequency of 12.5 kHz. All the samples were spun at the magic angle with a frequency of 14.0 kHz. Acquisition of the indirect dimension was synchronized with the rotors' spinning speed and for sampling in the t_1 dimension dwell times

of 18 to 36 µs were chosen. The data is shown after shearing transformation with sum projections of the high and low-resolution spectra along the *F*1 and *F*2 axis respectively. In order to obtain values of the second order quadrupole effect (*SOQE*) and the isotropic chemical shift (δ_{CS}^{iso}) the signal's center of gravity in *F*1 and *F*2 dimension was evaluated. Homonuclear ^{23}Na-^{23}Na dipole-dipole coupling strengths were determined by the static Hahn spin echo decay method [39]. Selective excitation of the central $m = 1/2 \leftrightarrow m = -1/2$ Zeeman transition was achieved using a ^{23}Na nutation frequency of 10.4 kHz for non-selective excitation, corresponding to π-pulse durations of about 24 µs for the solid samples. The homonuclear dipolar second moments $M_{2(Na-Na)}$ were determined from the Gaussian decay $I(2t_1)/I(0) = \exp(-2M_2t_1^2)$ at short evolution times ($2t_1 < 400$ µs). The experimental values were compared with those calculated from the closest Na−Na distances within the data range 0-30 Å [41, 42] in the crystal structures of NTP and NGP.

^{31}P-^{27}Al dipole-dipole interactions were measured using ^{27}Al{^{31}P} rotational echo double resonance (REDOR) and ^{31}P{^{27}Al} rotational echo adiabatic passage double resonance (REAPDOR) experiments [43]. The ^{31}P π-pulse length of 5.0 µs was adjusted by maximizing the difference signal Δ*S* at a fixed dephasing time and the ^{27}Al π-pulse length was 6.1 µs. Further, REAPDOR NMR experiments were performed at a rotor speed of 12.0 kHz, with a ^{31}P π/2 pulse length of 3.1 µs and a ^{27}Al adiabatic pulse duration of 27.8 µs. High resolution ^{27}Al and ^{31}P MAS NMR spectra were extracted and shown to allow a comparison of signal amplitudes without (S_0) and with (S) ^{31}P pulse irradiation after a dipolar mixing time of 16 rotor cycles.

Results and Discussion

Macroscopic properties

Figure 1 shows the DSC curves of the two series of glass samples investigated and the obtained glass transition temperatures are summarized in Table 1. The NATP glasses are distinguished by substantially higher T_g values compared to the NAGP glasses. In both series T_g and T_x tend to decrease with increasing Al content. Glassy NTP ($x = 0$) could not be obtained even by rapid quenching of the melt. The XRD powder patterns could be refined very well in the space group R−3c, despite the fact that pure NGP crystallizes in the (closely related) space group R−3. The lattice constants derived from these refinements are summarized in Table 2 and illustrated in Figure 3. While in the NAGP series the unit cell volume of the NASICON structure increases monotonically with increasing Al content, a

slight decrease in unit cell volume is observed for the NATP series. These variations may be understood taking into account that the ionic radius of Al^{3+} (0.535 Å) is larger than that of Ge^{4+} (0.530 Å) but smaller than that of Ti^{4+} (0.605 Å) [44].

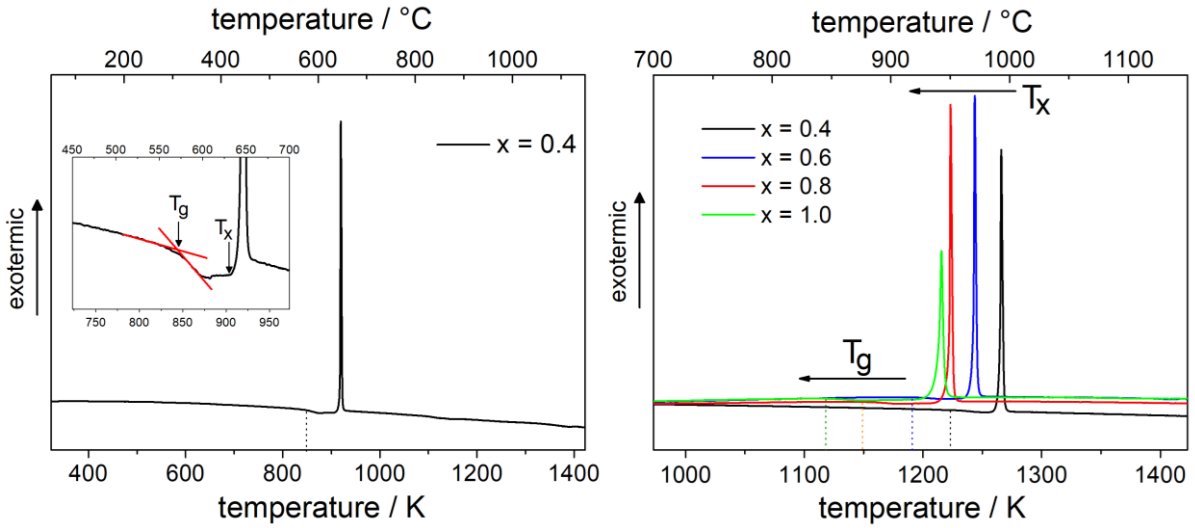

Figure 1: DSC data of a representative sample in the system $Na_{1+x}Al_xGe_{2-x}(PO_4)_3$ (left x = 0.4) and the $Na_{1+x}Al_xTi_{2-x}(PO_4)_3$ series (right). The vertical expansion illustrates the tangent method for obtaining the glass transition temperatures T_g.

In both series, the compositional dependence of lattice constants weakens for x-values above 0.8, indicating an approach to the solubility limit of the NASICON structure near this composition, and at higher x-values, the XRD data show evidence of secondary phases.

Table 1: Sample compositions, glass transition temperatures T_g, crystallization onset temperatures T_x, of glassy $Na_{1+x}Al_xGe_{2-x}(PO_4)_3$ and $Na_{1+x}Ti_xGe_{2-x}(PO_4)_3$ and densities for the respective glasses (ρ_{glass}) and glass-ceramics ($\rho_{cryst.}$). Indicated errors correspond to the standard deviation of 10 measurements of the same sample.

x	T_g / K ± 1 K		T_x / K ± 1 K		ρ_{glass} / g cm^{-3} ± 0.02 g cm^{-3}		$\rho_{cryst.}$ / g cm^{-3} ± 0.02 g cm^{-3}	
	NAGP	NATP	NAGP	NATP	NAGP	NATP	NAGP	NATP
0.0	884	-	939	-	3.34	2.85	3.36	2.99
0.4	843	950	918	992	3.16	2.82	3.21	2.95
0.6	833	918	917	970	3.06	2.80	3.16	2.85
0.8	813	876	919	949	2.97	2.76	3.05	2.85
1.0	794	845	919	940	2.91	2.73	2.98	2.82

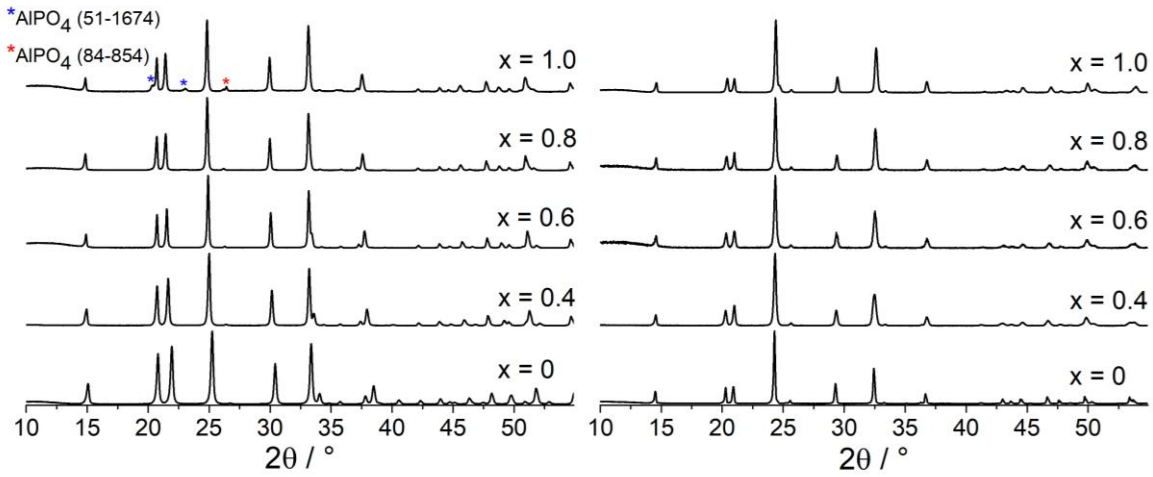

Figure 2: Powder diffraction patterns for $Na_{1+x}Al_xGe_{2-x}(PO_4)_3$ (left) and $Na_{1+x}Al_xTi_{2-x}(PO_4)_3$ (right) glass-ceramics. Diffraction peaks originating from impurity phases are marked with asterisks.

Table 2: Experimentally obtained lattice constants a (= b) and c for $Na_{1+x}Al_xGe_{2-x}(PO_4)_3$ and $Na_{1+x}Al_xGe_{2-x}(PO_4)_3$ glass ceramics refined in the hexagonal space group $R\bar{3}c$.

x	***a* (Å)**		***c* (Å)**	
	NAGP	NATP	NAGP	NATP
0.0	8.01	8.48	21.50	21.78
0.4	8.21	8.46	21.46	21.82
0.6	8.25	8.45	21.41	21.75
0.8	8.28	8.46	21.38	21.69
1.0	8.29	8.46	21.37	21.60

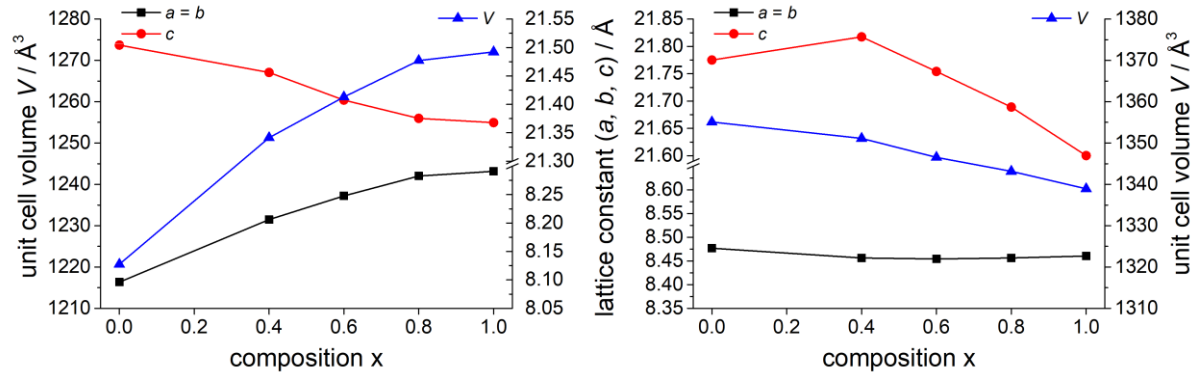

Figure 3: Lattice constants and unit cell volumes V for $Na_{1+x}Al_xGe_{2-x}(PO_4)_3$ (left)and $Na_{1+x}Al_xTi_{2-x}(PO_4)_3$ (right) glass ceramics refined in the hexagonal space group $R\bar{3}c$.

^{31}P MAS-NMR

^{31}P MAS NMR spectra of the vitreous $Na_{1+x}Al_xGe_{2-x}(PO_4)_3$ and $Na_{1+x}Al_xTi_{2-x}(PO_4)_3$ samples are displayed in Figure 4 and show broad, slightly asymmetric resonance lines, representing a distribution of ^{31}P isotropic chemical shifts. This inhomogeneous line broadening may arise from variations in the number of germanium, aluminum, and/or titanium next-nearest neighbors. Comparison of the average ^{31}P isotropic chemical shift (−29 ppm) measured in glassy NGP with the peak assignments previously made for $(Na_2O)_{0.33}[(2GeO_2)_x(P_2O_5)_{1-x}]_{0.66}$ (x = 0.4) glasses [45] suggests that the dominant phosphate species are comprised of $P^{(3)}_{nGe}$ ($1 \leq n \leq 3$) units, and possibly some $P^{(2)}_{0Ge}$ units.

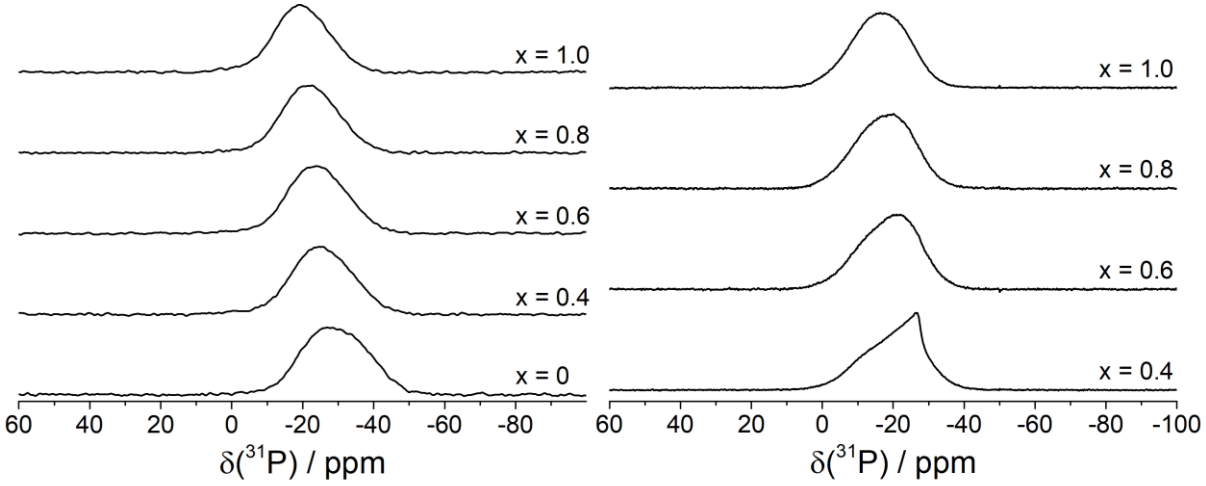

Figure 4: ^{31}P MAS NMR spectra of vitreous $Na_{1+x}Al_xGe_{2-x}(PO_4)_3$ (left) and $Na_{1+x}Al_xTi_{2-x}(PO_4)_3$ (right) at a carrier frequency of 98.13 MHz and MAS rate of 10.0 kHz.

With increasing Al content, the signals' full widths at half maximum (FWHM) decrease from 2400 Hz to 1900 Hz for the NAGP system and remain nearly constant around 2000 Hz for the NATP system, see Table 3. A sharp feature near −26.4 ppm for the x = 0.4 NATP sample suggests incomplete vitrification. In both systems, substitution of germanium and titanium by aluminum shifts the ^{31}P centers of gravity to higher frequencies. This trend can be explained in terms of the expected systematic increase in the number of Al next nearest neighbors present in the coordination sphere of phosphorus as x increases. In the NAGP system this compositional dependence is more pronounced than in the NATP system, indicating that ^{31}P chemical shifts respond more sensitively towards replacement of Ge by Al than by Ti in the second coordination sphere of the phosphate species.

Table 3: Centers of gravity δ_{CS}^{iso} and full width at half maximum, *FWHM*, of ^{31}P resonances in glassy $Na_{1+x}Al_xGe_{2-x}(PO_4)_3$ and $Na_{1+x}Al_xTi_{2-x}(PO_4)_3$.

x	**δ_{CS}^{iso} / ppm ± 0.5 ppm**		***FWHM* / Hz ± 40 Hz**	
	NAGP	NATP	NAGP	NATP
0	−29.0	-	2400	-
0.4	−25.5	−19.5	2100	2050*
0.6	−24.5	−19.3	2050	2000
0.8	−21.8	−17.8	2000	2000
1.0	−19.5	−16.3	1900	2000

*glassy component only

^{31}P MAS NMR spectra of crystallized $Na_{1+x}Al_xGe_{2-x}(PO_4)_3$ and $Na_{1+x}Al_xTi_{2-x}(PO_4)_3$ glass-ceramics are shown in Figure 5. The crystallized NAGP samples show partially resolved spectra, reflecting ^{31}P species with mixed ligation to germanium and aluminum. The results are quite analogous to those obtained in the corresponding Li-based system [11], except that in the present samples the amount of Al that can be incorporated into the NASICON structure is significantly higher. Even so, NAGP samples with x = 0.8 and 1.0 reveal sizeable fractions of remaining glassy material, as indicated by a broad signal near −10 ppm. The fraction of crystalline NAGP could not be increased by extending the annealing period up to 24 h or by increasing the annealing temperatures to 800 °C (data not shown). In the latter case, we observed partial sample decomposition. In contrast in the NATP system complete crystallization could be achieved by annealing for 30 min at 645 °C. Table 4 summarizes the results from the spectral deconvolution. In crystalline $NaGe_2(PO_4)_3$ the ^{31}P resonance at an isotropic chemical shift of about −38.0 ppm can be assigned to a tetrahedral phosphate site connected to four germanium ligands (P^4_{4Ge}). In $NaTi_2(PO_4)_3$ the signal of the corresponding P^4_{4Ti} site is observed at −27.0 ppm. With increasing extent of Al substitution, increasing concentrations of additional phosphate species of type $P^4_{nAl,(4-n)X}$ ($0 \le n \le 4$; X = Ge,Ti) are expected. In the NAGP system the isotropic chemical shifts of these sites depend systematically on n. These sites give rise to partially overlapping signals in the −25 to −45 ppm region. Most notably, Table 4 shows that in most of the samples the fractional areas obtained from this deconvolution analysis are in excellent agreement with the prediction based on a random substitution of Ge by Al, (binomial distribution) [11,46]. Only for the highest Al contents some systematic deviations are notable, which can be attributed to the formation of the secondary phase $AlPO_4$. In the NATP system (Figure 5, right) no such a clear

shift distinction is seen for the individual $P^{(4)}_{(4-n)Ti,nAl}$ sites. Evidently, in this system the ^{31}P chemical shift turns out to be much less sensitive to changes in the second coordination sphere of the phosphate species. This lack of chemical shift discrimination may be understandable in terms of the trends in the lattice constants. While substitution of Ge^{4+} with Al^{3+} leads to a substantial expansion of the lattice, reflecting the need to accommodate the additional Na^{+} ions, the situation is different in the NATP system, where substitution of Ti^{4+} by Al^{3+}, although aliovalent, causes much less structural perturbation. Here it seems that replacing the Ti^{4+} ions by the smaller Al^{3+} species can counterbalance the expansion associated with the accommodation of the additional Na^{+} ions effectively. Nevertheless, the gradual shift in the center of gravity of the ^{31}P signals appears to be consistent with a binomial distribution of local $P^{(4)}_{(4-n)Ti,nAl}$ environments in the NTP lattice.

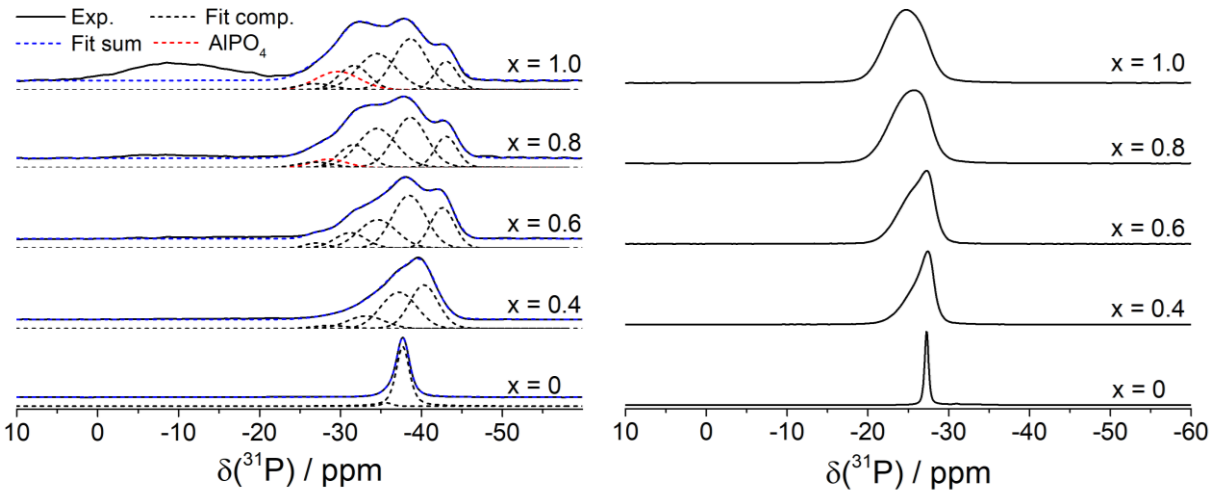

Figure 5: ^{31}P MAS NMR spectra of crystalline $Na_{1+x}Al_xGe_{2-x}(PO_4)_3$ (left) and $Na_{1+x}Al_xTi_{2-x}(PO_4)_3$ (right) at a carrier frequency of 98.13 MHz and a MAS rate of 10.0 kHz. The deconvolution component shown in red arises from crystalline $AlPO_4$.

The assignment of the observed lines to the individual species is confirmed with help of $^{31}P\{^{27}Al\}$ REAPDOR experiments, conducted on the Ge-containing samples of compositions x = 0.8 and x = 1.0, see Figure 6. The ^{31}P MAS-NMR spectra are shown with and without dipolar recoupling at a fixed dipolar mixing time. Owing to the dipolar recoupling occurring in the mixing time of the $^{31}P\{^{27}Al\}$ REAPDOR experiment, the ^{31}P signal intensity is successively diminished as the number of aluminum ligands to phosphorus (n) increases. The weakest REAPDOR effect is observed for the resonances at around −41 to −44 ppm, which can thus be attributed to P^4_{4Ge} units.

Table 4: Deconvolution parameters center of gravity δ and *FWHM* for the ^{31}P MAS NMR spectra of $Na_{1+x}Al_xTi_{2-x}(PO_4)_3$ glass-ceramics and isotropic chemical shifts δ_{CS}^{iso}, *FWHM* and area fraction of the resolved components in the $Na_{1+x}Al_xGe_{2-x}(PO_4)_3$ glass-ceramics spectra. Area fractions omit glassy phases for compositions marked with an asterisk. x-values deduced from the peak deconvolutions assuming binomial distributions, denoted x_{real}, are shown in parentheses in the first column

x (x_{real})	**δ/ ppm ± 0.5 ppm**	***FWHM* / Hz ± 40 Hz**	**P^4_{nAl} Species**	**δ_{CS}^{iso} / ppm ± 0.5 ppm**	***FWHM* / Hz ± 40 Hz**	**Area fraction / % ± 2%**	
	NATP	NATP	NAGP	NAGP	NAGP	Calc.	Exp.
0.4	−26.5	440	P^4_{0Al}	−40.3	410	41.0	41
(0.41)			P^4_{1Al}	−37.2	510	41.0	41
			P^4_{2Al}	−33.1	540	15.3	15
			P^4_{3Al}	−28.7	500	2.5	3
			P^4_{4Al}	-	-	0.2	-
0.6	−26.0	680	P^4_{0Al}	−42.6	340	24.0	22
(0.66)			P^4_{1Al}	−38.5	480	41.2	40
			P^4_{2Al}	−34.6	540	26.5	24
			P^4_{3Al}	−31.2	440	7.5	11
			P^4_{4Al}	−27.0	310	0.8	3
0.8*	−25.3	870	P^4_{0Al}	−43.0	310	12.4	14
(0.79)			P^4_{1Al}	−38.6	470	33.2	33
			P^4_{2Al}	−34.5	550	33.2	30
			P^4_{3Al}	−31.7	430	14.7	13
			P^4_{4Al}	−26.8	510	2.5	4
			$AlPO_4$	−28.6	490	4.0	6
1.0*	−24.9	912	P^4_{0Al}	−43.1	310	5.3	11
(0.8)			P^4_{1Al}	−38.7	490	21.0	32
			P^4_{2Al}	−34.5	550	31.6	26
			P^4_{3Al}	−31.7	430	21.0	13
			P^4_{4Al}	−26.9	510	5.3	4
			$AlPO_4$	−29.7	620	15.6	14

*glassy phases: x = 0.8: δ_{CS}^{iso} = −9.4 ppm – area fraction 5%
x = 1.0: δ_{CS}^{iso} = −10.2 ppm – area fraction 23%

Signals at higher frequencies show a continuously stronger REAPDOR effect and are subsequently attributed to sites with higher *n* values. Furthermore, Figure 6 illustrates rather very weak ^{31}P-^{27}Al dipolar couplings for the residual glass, indicating that very little aluminum remains in the residual glass phase after crystallization of the x = 1.0 sample.

In the latter cases, the fraction of $AlPO_4$ obtained from the ^{27}Al MAS NMR data (see below) was used to calculate the expected $AlPO_4$ signal intensity in the ^{31}P spectra and taken into consideration in the spectral deconvolution. In this way, the real concentrations of aluminum and phosphorus present in the NASICON phase can be deduced. The theoretically calculated signal intensities based on the binomial distribution were corrected accordingly. Following this procedure, the ^{31}P NMR spectrum of the x = 0.8 ceramic sample was found in excellent agreement with the theoretically predicted spectrum. For the composition x = 1.0 however, the experimental intensity distribution deviates from the predicted one, suggesting that the composition of the NASICON phase corresponds to a value close to x = 0.8. This observation is also confirmed by calculation of the real compositions x_{real} following the expression [11]

$$\frac{Al^{3+}}{Ge^{4+}} = \frac{\sum_{n=0}^{4} nP_{nAl}^{4}}{\sum_{n=0}^{4}(4-n)P_{nAl}^{4}} = \frac{x_{real}}{2-x_{real}}$$

(see also Table 5) and is further supported by the small change in lattice parameters in going from x = 0.8 to x = 1.0. Again, we note that for the NAGP glass-ceramics with high aluminum content the crystallization is not complete, as the ^{31}P MAS-NMR spectra show about 5 % and 23 % of phosphorus atoms present in the residual glassy phase, for x = 0.8 and 1.0, respectively.

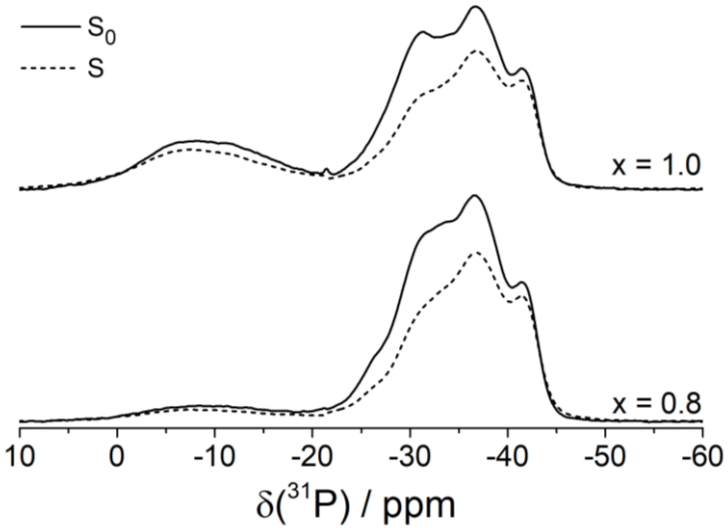

Figure 6: High resolution ^{31}P MAS NMR spectra from ^{31}P{^{27}Al} REAPDOR experiments for crystalline $Na_{1+x}Al_xGe_{2-x}(PO_4)_3$ with compositions x = 0.8 and x = 1.0. The spectra were recorded using a MAS frequency of 10.0 kHz and S_0 represents spectra for no dipolar mixing while spectra *S* are obtained after a dipolar mixing time corresponding to 16 rotor cycles.

^{27}Al MAS-NMR

The ^{27}Al MAS NMR spectra of the glassy materials (Figure 7) feature resonances attributable to aluminum in four-, five-, and six-coordination at isotropic chemical shifts around 46.7 ppm, 15.0 ppm and −10.3 ppm respectively. Analogous results were recently reported for related glasses of compositions $Li_{1+x}Al_xGe_{2-x}(PO_4)_3$ (LAGP) [11] and $Li_{1+x}Al_xSn_yGe_{2-(x+y)}(PO_4)_3$ (LA(Sn)GP) [10].

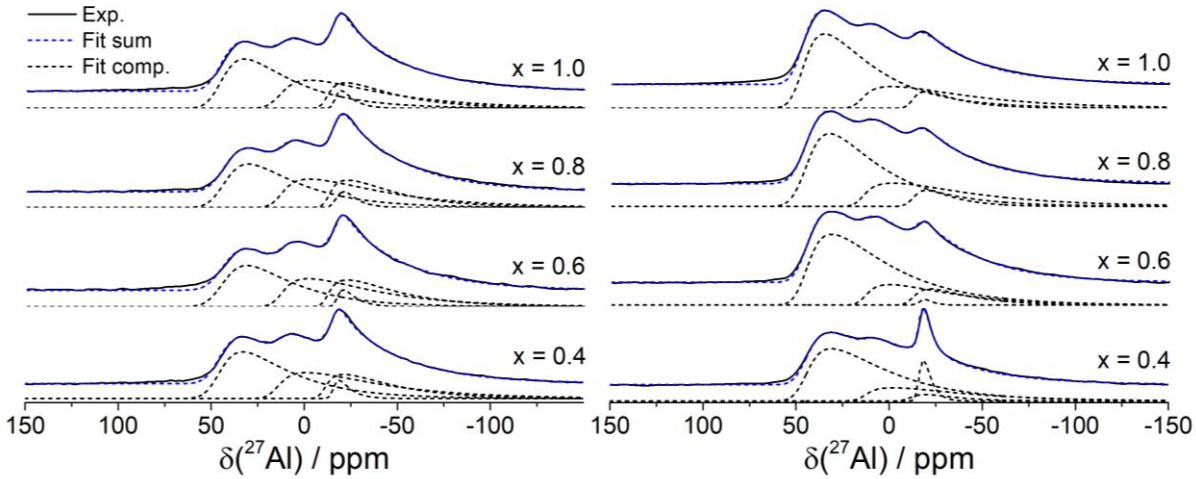

Figure 7: ^{27}Al MAS NMR spectra of vitreous $Na_{1+x}Al_xGe_{2-x}(PO_4)_3$ (left) and $Na_{1+x}Al_xTi_{2-x}(PO_4)_3$ (right) at a carrier frequency of 63.16 MHz and MAS rate of 14.0 kHz.

The signals show the characteristic lineshapes arising from second order quadrupole perturbations in the presence of a wide distribution of electric field gradients. To account for this broadening effect, we used the Czjzek model based on the statistical distribution of η_Q and C_Q values [37] for simulating these lineshapes. To arrive at a satisfactory fit, small area fractions of a fourth site near the isotropic chemical shift of Al^6_{cryst} had to be included (see Table 4). Note that the glassy NATP samples contain significantly more four-coordinated ^{27}Al species than the glassy NAGP samples. We expect the titanium atoms in the glassy state to be predominantly six-coordinated, whereas in the case of the glassy NAGP samples, previous results on related glasses in the Na_2O-GeO_2-P_2O_5 system suggest a distribution of germanium coordination numbers ranging from four to six [44]. Thus, it appears that the coordination distribution of aluminum depends on the preferred coordination number of the tetravalent metal atom in the glass. The same effect was previously observed in glassy LA(Sn)GP [10] samples, where the reported ^{119}Sn MAS NMR experiments show tin to be exclusively six-

coordinated in the glassy state and where a higher fraction of Al is found to be four-coordinated than for the Sn-free LAGP samples [11].

Contrary to vitreous NAGP and NATP samples, ^{27}Al MAS NMR spectra of the crystalline specimens (Figure 8) with low *x*-values feature only a single resonance at an isotropic chemical shift of about −14.5 ppm for NAGP and −17.5 ppm for NATP respectively, corresponding to six-coordinated sites in the NASICON structure.

Table 5: Simulation parameters for the ^{27}Al MAS NMR spectra using the Czjzek model for glassy $Na_{1+x}Al_xGe_{2-x}(PO_4)_3$ and $Na_{1+x}Al_xTi_{2-x}(PO_4)_3$ samples.

x	**Al species**	**δ_{CS}^{iso} / ppm ± 0.5 ppm**		**Average C_Q / MHz ± 0.1 MHz**		**Area fraction / % ± 2%**	
		NAGP	NATP	NAGP	NATP	NAGP	NATP
0.4	Al^4	47.3	46.2	4.3	4.7	43	68
	Al^5	15.7	14.3	5.2	5.2	33	20
	Al^6	−10.2	−10.5	4.2	3.4	20	4
	Al^6_{cryst}	−15.3	−15.9	2.0	1.6	4	8
0.6	Al^4	46.5	47.0	4.3	4.7	39	69
	Al^5	14.7	15.0	5.0	4.8	33	20
	Al^6	−10.7	−11.0	4.3	3.8	24	10
	Al^6_{cryst}	−16.4	−15.9	2.1	1.6	4	1
0.8	Al^4	45.8	47.3	4.4	4.4	40	64
	Al^5	15.0	16.5	5.2	5.4	34	28
	Al^6	−11.4	−11.1	4.2	3.2	22	8
	Al^6_{cryst}	−16.0	-	2.1	-	4	-
1.0	Al^4	47.3	49.0	4.3	4.3	42	64
	Al^5	17.0	17.0	5.2	5.4	34	27
	Al^6	−10.7	−10.7	4.2	3.4	20	9
	Al^6_{cryst}	−15.3	-	2.1	-	4	-

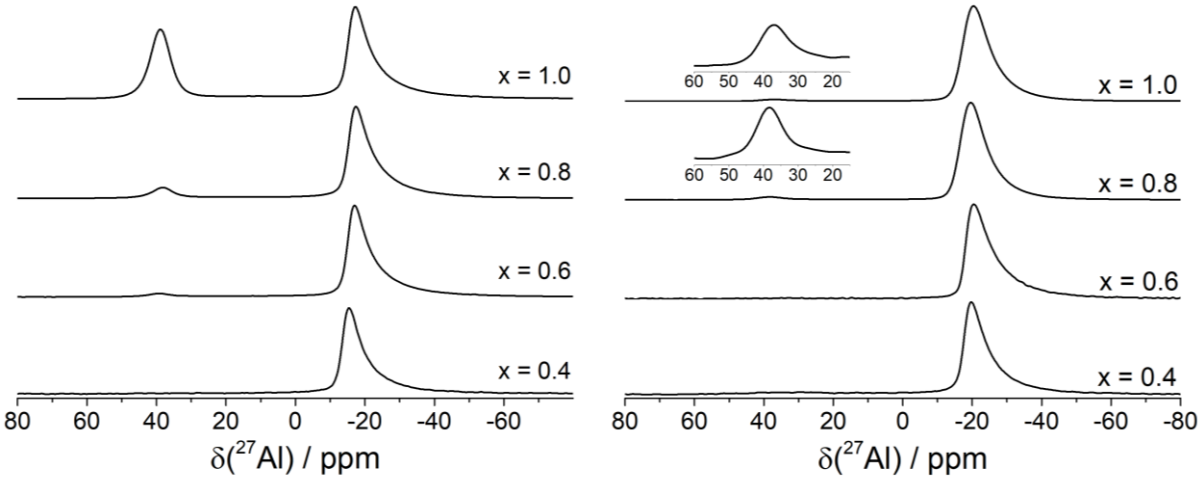

Figure 8: ^{27}Al MAS NMR spectra of crystalline $Na_{1+x}Al_xGe_{2-x}(PO_4)_3$ (left) and $Na_{1+x}Al_xTi_{2-x}(PO_4)_3$ (right) at a carrier frequency of 63.16 MHz and MAS spinning rate of 10.0 kHz. Vertical expansions showing low concentrations of $AlPO_4$ are included.

At higher substitution levels, a second resonance is observed at a chemical shift of about 37.0 ppm, attributable to the impurity phase $AlPO_4$. The latter peak is much more pronounced in the case of the NAGP samples, suggesting that the Al solubility in the Ge-NASICON lattice is more restricted. This decomposition process has also been observed in the Li-based system and explained by reaching the solubility limit of aluminum in the NASICON phase. In that system, the exact solubility limit and hence the extent of $AlPO_4$ formation is also influenced by the preparation method [11,28].

^{23}Na MAS NMR

Figure 9 shows the ^{23}Na MAS NMR spectra of glassy NAGP and NATP samples exhibiting broad, asymmetric signals. All the spectra can be excellently modeled by a simulation of a single component according to the Czjzek model resulting in δ_{CS}^{iso} values around −9.5 and −12.9 ppm along with C_Q values of 2.6 and 2.5 MHz for NAGP and NATP respectively. The ^{23}Na isotropic chemical shift of glassy NGP is close to that measured in the compositionally related $(Na_2O)_{0.33}[(2GeO_2)_x(P_2O_5)_{1-x}]_{0.66}$ (x = 0.4) glass (−8.3 ppm) [45], again suggesting a similar local environment governed by anionic germanate and phosphate species. Within each system's composition range, the variations in isotropic chemical shift values and *FWHM* are small, however.

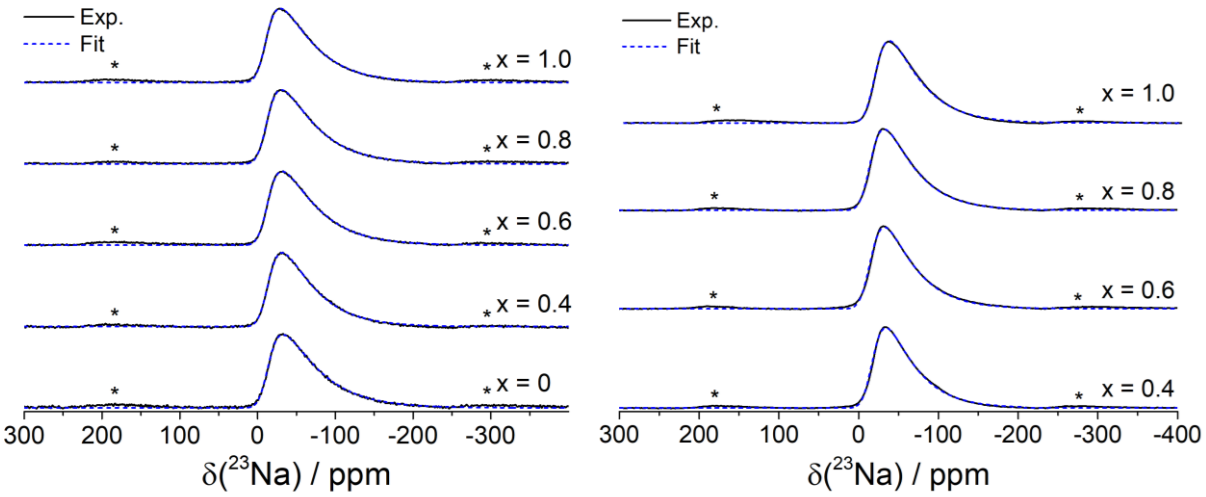

Figure 9: ^{23}Na MAS NMR spectra of vitreous $Na_{1+x}Al_xGe_{2-x}(PO_4)_3$ (left) and $Na_{1+x}Al_xTi_{2-x}(PO_4)_3$ (right) at a carrier frequency of 64.12 MHz and MAS rate of 15.0 kHz. Spinning sidebands are marked with an asterisk.

In the NASICON structure (Figure 10) sodium ions can principally occupy a site Na1 in distorted octahedral (trigonal antiprismatic) coordination or an eight- to ten-coordinated interstitial sodium site Na2. Further, in the crystal structure of NGP, half of all Na1 sites are replaced by a closely related Na1' site showing distorted octahedral (trigonal prismatic) coordination. This second site arises as a result of two distinguishable GeO_6 octahedra and can be visualized by rotating either one Ge octahedron, shown in Figure 10c, by 60° about the lattice's *c*-axis.

Table 6: Isotropic chemical shifts δ_{CS}^{iso} and average quadrupolar coupling constants C_Q of the ^{23}Na resonances in glassy $Na_{1+x}Al_xGe_{2-x}(PO_4)_3$ (NAGP) and $Na_{1+x}Al_xTi_{2-x}(PO_4)_3$ (NATP).

Composition	**δ_{CS}^{iso} / ppm**		**Average C_Q / kHz**	
x	**± 0.5 ppm**		**± 100 kHz**	
	NAGP	NATP	NAGP	NATP
0	−10.4	-	2700	-
0.4	−10.5	−14.8	2600	2400
0.6	−9.8	−12.2	2600	2450
0.8	−9.0	−12.0	2600	2450
1.0	−7.8	−12.5	2800	2500

Previous work by $^{6/7}$Li NMR on the analogous LAGP system has shown that both the chemical shift and nuclear electric quadrupolar coupling parameters are potentially useful to differentiate between differently coordinated crystal sites [11]. Figure 11 show the

corresponding ^{23}Na MAS NMR spectra of pure NGP and NTP. For both compositions, the spectra show no more sodium species in the glassy state, suggesting that the crystallization has been complete.

The spectrum of NTP can be simulated with a single central transition MAS powder pattern characterized by an isotropic chemical shift of −7.1 ppm, a quadrupole coupling constant of C_Q = 2.93 MHz and a very small asymmetry parameter of η_Q = 0.01, in relatively good agreement with TQMAS data (see Table 6, Table 7 and Figure 11). We attribute this signal to sodium ions occupying the "regular" Na1 sites. In contrast, Figure 11 shows further that the spectrum of NGP is significantly more complex. We can identify three different ^{23}Na MAS NMR signals, in agreement with TQMAS data (Figure 12). Two of them have rather similar quadrupole coupling constants and asymmetry parameters. In addition, small amounts (4%) of a sodium species with a low electric field gradient (4%) at an isotropic chemical shift of −37.4 ppm can be noted. This species might arise from a particular defect site in which the sodium ions appear to have significant ionic mobility. The spectroscopic differences between NTP and NGP are not surprising, as they are not isomorphous.

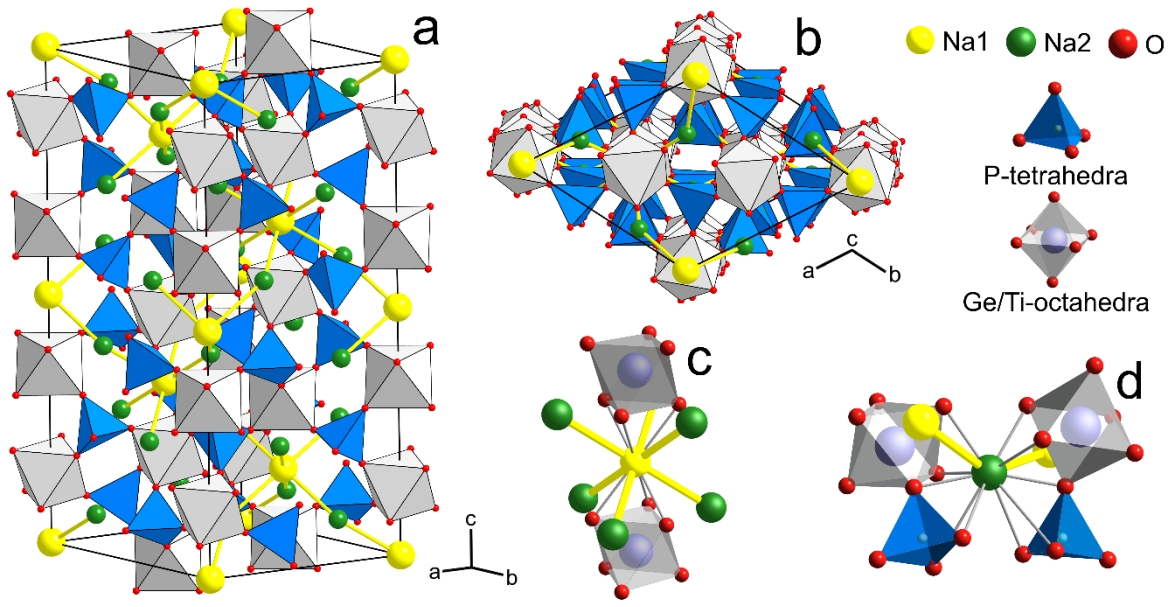

Figure 10: Representation of the NASICON unit cell (a,b) and Na-coordination geometries of the Na1 (c) and Na2 site (d) further showing the bottleneck of Na-ion pathways through the crystal structure.

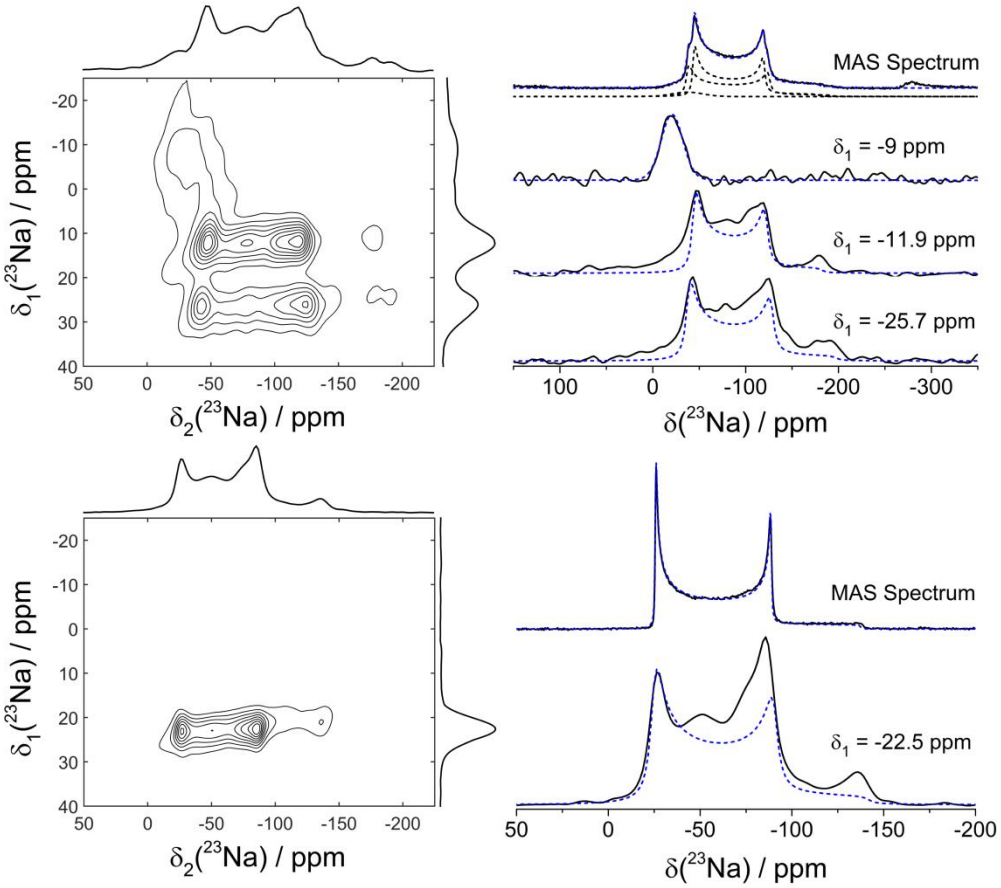

Figure 11: ^{23}Na TQMAS spectra of $NaGe_2(PO_4)_3$ (top left) and $NaTi_2(PO_4)_3$ (bottom left). Included are "slices" showing the spectra in the F_2 domain correlated with the peak maxima observed in the F_1 domain. The experimental MAS NMR data are also included. Dashed curves represent simulated spectra, using the parameters listed in Table 6.

Table 7: Fit Parameters obtained from the ^{23}Na MAS NMR and TQMAS experiments of crystalline $NaGe_2(PO_4)_3$.

Comp.	**Site**	**δ_{CS}^{iso} / ppm ± 0.5 ppm**	***FWHM* / Hz ± 40 Hz**	**C_Q / kHz ± 0.1 kHz**	**η**	**Area fraction / % ± 2%**
NGP	1 (MAS)	−11.5	-	3450	0.01	42
x = 0	2 (MAS)	−21.7	-	3200	0.02	54
	3 (MAS)	−37.4	2500	-	-	4
	1 (TQMAS)	−11.6	-	3500	0.01	-
	2 (TQMAS)	−21.5	-	3250	0.02	-
	3 (TQMAS)	−20.7	1760	-	-	-

Table 8: Fit Parameters obtained from the ^{23}Na MAS NMR and TQMAS experiments of crystalline $NaTi_2(PO_4)_3$ and $Na_{1+x}Al_xTi_{2-x}(PO_4)_3$ samples.

Comp.	Experiment	δ_{CS}^{iso} / ppm ± 0.5 ppm	C_Q / kHz ± 0.1 kHz	η_Q (±0.05)
$x = 0$	MAS	−7.1	2930	0.01
x = 0	TQMAS	−5.1	2970	0
x = 0.4	MAS	−12.6	2980	0.14
x = 0.6	MAS	−14.2	3040	0.25
x = 0.8	MAS	−19.9	3030	0.36
x = 1.0	MAS	−20.7	3050	0.40

Figure 12 summarizes the MAS-NMR spectra of both $Na_{1+x}Al_xGe_{2-x}(PO_4)_3$ and $Na_{1+x}Al_xTi_{2-x}(PO_4)_3$ as a function of substitution level *x*. The spectra show increasingly significant line broadening effects, both in MAS and TQMAS spectra, suggesting that the disorder created by Al/Ge and Al/Ti substitution along with the accommodation of additional Na^+ ions creates a wide distribution of isotropic chemical shifts and/or nuclear electric quadrupole coupling constants. Owing to the complexity of these spectra no unambiguous fits could be obtained for the NAGP series (and are thus not shown), even when taking recourse to additional TQMAS data. The spectra of the NATP series could be simulated by including a line broadening parameter and by artificially increasing the η_Q value (which affects the shape of second-order quadrupolar spectra in a similar way as a distribution of quadruolar coupling constants). Qualitatively, Figure 12 suggests that the aliovalent substitution modifies the sodium local environments more strongly in the NAGP system than in the NATP system. This finding is consistent with the much smaller effect of the Al/Ti substitution upon the ^{31}P NMR chemical shifts compared to the Al/Ge substitution. Again, these effects can be understood in terms of the significant difference in unit cell parameters and volumes between both systems.

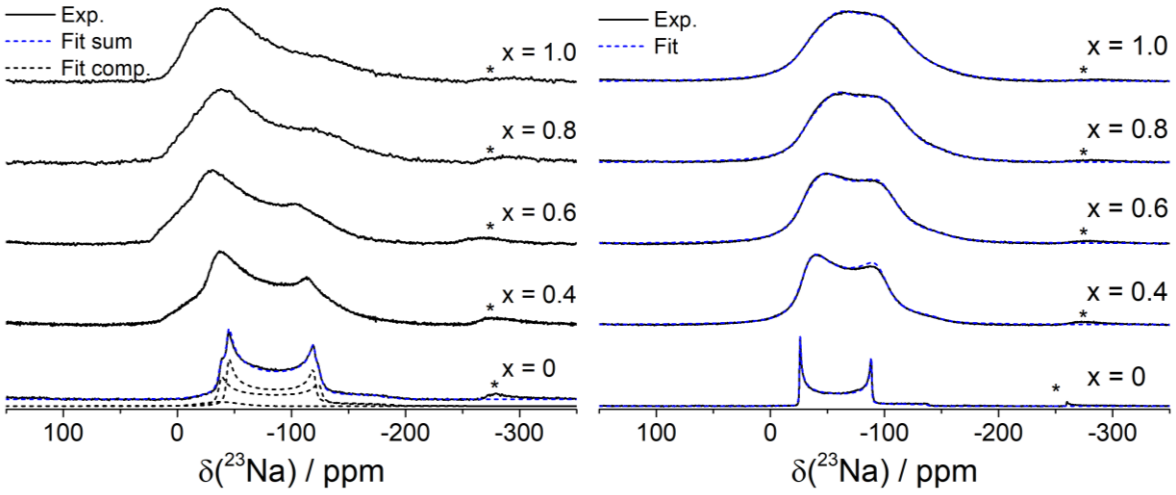

Figure 12: ^{23}Na MAS NMR spectra of crystalline $Na_{1+x}Al_xGe_{2-x}(PO_4)_3$ (left) and $Na_{1+x}Al_xTi_{2-x}(PO_4)_3$ (right) at a carrier frequency of 64.119 MHz and MAS rate of 15.0 kHz. Spinning sidebands are marked with an asterisk. In the case of the NATP system, simulated spectra (dotted curves) are superimposed on the experimental data.

^{23}Na spin echo decay spectroscopy

Finally, Figure 13 compares results from ^{23}Na spin echo decay spectroscopy for the glassy and crystalline compounds. From the internuclear distance distribution in the crystal structures we expect $M_{2(Na-Na)}$ values of 0.54×10^6 rad^2 s^{-2} and 0.43×10^6 rad^2 s^{-2} in NGP and NTP, respectively.

The decay obtained for crystalline NTP is Gaussian over the entire measurement range ($2t_1$ < 1000 µs) leading to an $M_{2(Na-Na)}$ value of 0.55×10^6 rad^2 s^{-2} in reasonable agreement with the crystal structure. In contrast, the spin echo decay of crystalline NGP shows some deviations from Gaussian character, suggesting a distribution of $M_{2(Na-Na)}$ values. Fitting the data over the entire data range ($2t_1$ <1000 µs), values of 0.58×10^6 rad^2 s^{-2} and 0.66×10^6 rad^2 s^{-2} are obtained at 300 and 200 K, respectively, which are in excellent agreement with the theoretical value. An improved Gaussian fit with a somewhat larger M_2 value of 0.85×10^6 rad^{2}s^{-2} at 300 K can be obtained if one restricts the analysis over a smaller range of dipolar evolution times ($2t_1$ < 400 µs). Evidently the sodium ion distribution in this material is somewhat inhomogeneous, which might be related to the presence of the third site in the MAS NMR spectra.

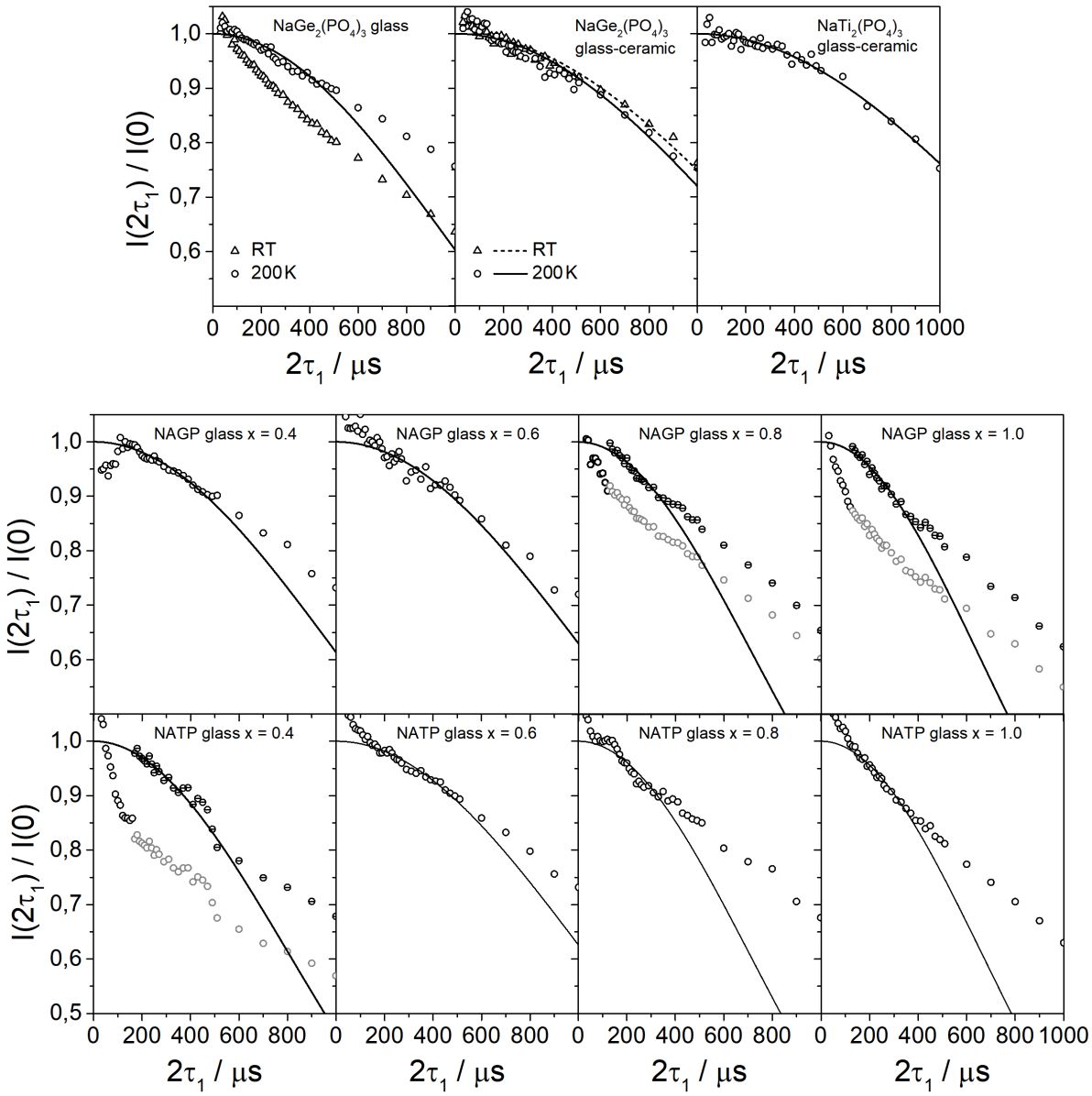

Figure 13: Top: Normalized ^{23}Na spin-echo amplitudes as a function of delay time 2τ for crystalline $NaTi_2(PO_4)_3$ (left), crystalline $NaGe_2(PO_4)_3$ (center) and its glass (right).
Bottom: Normalized ^{23}Na spin-echo amplitudes as a function of delay time 2τ for glassy NAGP and NATP samples. In those cases where bimodal spin echo decays were found, the data of the slower decay component are plotted in a re-normalized fashion.

In the case of glassy NGP, we find that the room temperature spin echo decays are substantially steeper and of approximately exponential character, suggesting a dynamic contribution to the spin-spin relaxation times due to sodium ionic motion. By lowering the measurement temperature to 200 K we were able to suppress this contribution, however, still substantial deviations from Gaussian decays are observed. Such deviations are the expected consequence of a distribution of dipolar coupling strengths, arising from a statistical spatial distribution of sodium ions in the glassy state. As a result of these distortions, the errors in M_2

are estimated at 20%, rather than 10% in crystalline NGP and NTP. An approximate fit over the initial data range $2t_1 < 510\,\mu s$ yielded an $M_{2(Na-Na)} = 1.0 \times 10^6\,rad^2\,s^{-2}$ at 163 K. This value is somewhat higher than the one measured in the isochemical crystal, suggesting the occurrence of Na−Na distances in the glassy state that are shorter than in the crystalline material. Table 9 summarizes the $M_{2(Na-Na)}$ values as a function of x for both the NAGP and the NATP glasses, by approximating the spin echo decays to Gaussians in an analogous manner as done in Figure 13a. In some cases additional very steep decays were observed in the region of short evolution times, the origins of which are not clear at the present time. Table 9 also includes the data ranges over which the M_2 values were obtained. As expected, the results for NATP and NAGP glasses are very similar, showing the expected tendency of $M_{2(Na-Na)}$ values to increase with increasing sodium content of the glasses. The average second moment of NGP glass can be compared to values between 2.8×10^6 and 4.3×10^6 $rad^2\,s^{-2}$ in $(Na_2O)_{0.33}[(2GeO_2)_x(P_2O_5)_{1-x}]_{0.66}$ glasses [45], where the Na ions are more concentrated than in NGP glass. For the crystallized NAGP and NATP samples, no meaningful $M_{2(Na-Na)}$ values could be obtained. In those samples Al-containing samples the enhanced sodium ionic mobility produces a substantial dynamic contribution to the spin-spin relaxation behavior, even at reduced temperatures. As result the spin echo decays of those materials cannot be analyzed in terms of magnetic dipole-dipole interactions.

Table 9: Dipolar second moment values $M_{2(Na-Na)}$ in crystalline NGP and NTP and in glassy NAGP and NATP samples.

	NAGP	NATP
Glass Composition	M_2 / rad²/s²	M_2 / rad²/s²
Glass-Ceramic x = 0	0.66±0.07 (0 - 1000)	0.55±0.06 (0 - 1000)
x = 0	1.0±0.2 (0 - 510)	-
x = 0.4	1.0±0.2 (130 - 470)	1.2±0.2 (170 -470)
x = 0.6	0.9±0.2 (130 - 470)	0.9±0.2 (130 - 470)
x = 0.8	1.9±0.4 (130 - 370)	2.0±0.4 (130 - 370)
x = 1.0	2.4±0.4 (130 - 370)	2.3±0.4 (130 - 370)

Conclusions

NASICON type ion-conducting glass-ceramics of NAGP and NATP solid solutions can be obtained by thermal treatment of isochemical base glasses. The glass-to-crystal transition was

studied by XRD and multinuclear single and double resonance NMR experiments. ^{31}P MAS NMR experiments show that $P^{(3)}$ species (three bridging oxygen atoms) connected to four, five and six coordinated Ge and Al dominate the structure of the glassy samples, whereas the local environments in the crystalline state are of the $P^{(4)}$ type (four bridging oxygens). Both glass systems differ significantly with respect to the coordination distribution of the tetravalent ions, which also affects the average coordination number of aluminum as quantified by ^{27}Al MAS NMR. Crystallization has the effect of ordering both elements' local environments in a manner that the crystalline state exhibits aluminum species in solely six coordination and $P^{(4)}$ species with varying numbers of Ge and Al ligands subjected to a binomial distribution. ^{23}Na NMR data obtained on glassy and crystalline NGP also indicate substantial changes in the spatial distribution of the sodium ions upon crystallization. While in the crystalline materials the sodium ions are uniformly distributed, in the isochemical glass the results are most consistent with a random spatial distribution of the sodium ions, which produces strongly non-Gaussian spin echo decays. Overall, the structural perturbations caused by aliovalent substitution and accommodation of additional sodium ions are significantly stronger in the NAGP system than in the NATP system. This effect may be related to the substantial difference in lattice parameters and unit cell volumes of the NASICON base structures (see Table 2).

Acknowledgements:

This work was funded by the FAPESP process No. 2013/07793-6 via the CEPID program. H.B. also thanks the Deutsche Forschungsgemeinschaft for financial support.

References

[1] V. Etacheri, R. Marom, R. Elazari, G. Salitra, D. Aurbach, *Energy Environ. Sci.* 4 (2011), 3243.

[2] B. Scrosati, J. Hassoun, Y.-K. Sun, *Energy Environ. Sci.* 4 (2011), 3287.

[3] D. Kundu, E. Talaie, V. Duffort, L. F. Nazar, *Angew. Chemie - Int. Ed.* 54 (2015), 3432.

[4] A. Manthiram, X. Yu, S. Wang, *Nat. Rev. Mater.* 2 (2017), 16103.

[5] J. G. Kim, B. Son, S. Mukherjee, N. Schuppert, A. Bates, O. Kwon, M. J. Choi, H. Y. Chung, S. Park, *J. Power Sources* 282 (2015), 299.

[6] N. Anantharamulu, K. Koteswara Rao, G. Rambabu, B. Vijaya Kumar, V. Radha, M. Vithal, *J. Mater. Sci.* 46 (2011), 2821.

[7] J. Fu, *Solid State Ionics* 96 (1997), 195.

[8] J. C. Bachman, S. Muy, A. Grimaud, H.-H. Chang, N. Pour, S. F. Lux, O. Paschos, F. Maglia, S. Lupart, P. Lamp, et al., *Chem. Rev.* 116 (2016), 140.

[9] B. E. Francisco, C. R. Stoldt, J. C. M'Peko, *J. Phys. Chem. C* 119 (2015), 16432.

[10] S. H. Santagneli, H. V. A. Baldacim, S. J. L. Ribeiro, S. Kundu, A. C. M. Rodrigues, C. Doerenkamp, H. Eckert, *J. Phys. Chem. C* 120 (2016), 14556.

[11] C. Schröder, J. Ren, A. C. M. Rodrigues, H. Eckert, J. Phys. Chem. C. 118 (2014), 9400.

[12] J. L. Narváez-Semanate, A. C. M. Rodrigues, *Solid State Ionics* 181 (2010), 1197.

[13] V. Diez-Gómez, K. Arbi, J. Sanz, *J. Am. Chem. Soc.* 138 (2016), 9479.

[14] M. Kaus, M. Guin, M. Yavuz, M. Knapp, F. Tietz, O. Guillon, H. Ehrenberg, S. Indris, *J. Phys. Chem. C* 121 (2017), 449.

[15] H. Xie, Y. Li, J. B. Goodenough, *RSC Adv.* 1 (2011), 1728.

[16] I. Y. Pinus, A. V. Khoroshilov, K. S. Gavrichev, V. P. Tarasov, A. B. Yaroslavtsev, *Solid State Ionics* 212 (2012), 112.

[17] M. Barré, J. Emery, P. Florian, F. Le Berre, M.-P. Crosnier-Lopez, J.-L. Fourquet, *J. Phys. Condens. Matter* 21 (2009), 175404.

[18] B. Lang, B. Ziebarth, C. Elsässer, *Chem. Mater.* 27 (2015), 5040.

[19] Q. Zhang, Z. Wen, Y. Liu, S. Song, X. Wu, *J. Alloys Compd.* 479 (2009), 494.

[20] F. E. Mouahid, M. Bettach, M. Zahir, P. Maldonado-Manso, S. Bruque, E. R. Losilla, M. A. G. Aranda, *J. Mater. Chem.* 10 (2000), 2748.

[21] Y.S. Zhu, L.L. Li, C.Y. Li, L. Zhou, ,Y.P. Wu, *Solid State Ionics* 289 (2016), 113.

[22] D. R. M. S. Wong, P. J. Newman, A. S. Best, K. M. Nairn, M. Forsyth, *J. Mater. Chem.* 8 (1998), 2199.

[23] H. Eckert, A.C.M. Rodrigues, *Mater. Res. Soc. Bull.* 42 (2017), 206.

[24] Z. Liu, S. Venkatachalam, L. van Wüllen, *Solid State Ionics* 276 (2015), 47.

[25] Z. Liu, S. Venkatachalam, H. Kirchhain, L. van Wüllen, *Solid State Ionics* 295 (2016) 32.

[26] K. Arbi, S: Mandal, J. M. Rojo, J. Sanz, *Chem. Mater.* 14 (2002), 1091.

[27] K. Arbi, W Bucheli, R. Jimenez, J. Sanz, *J. Eur. Ceram. Soc.* 35 (2015), 1477.

[28] K.Arbi, M. Tabellout, M. G. Lazarraga, J. M. Rojo, J. Sanz, *Phys. Rev B* 72 (2005), 094302.

[29] K.Arbi, M. A. Paris, J. Sanz, *Dalton Trans.* 40 (2011), 10195.

[30]. E. R. Losilla, M. A. G. Aranda, S. Bruque, J. Sanz, M. A. Paris, J. Campo, A. R. West,

Chem. Mater. 12 (2000), 2134.

[31] R. Losilla, M. A. G. Aranda, S. Bruque, *Chem. Mater.* 10 (1998), 665.

[32] A. Altomare, N. Corriero, C. Cuocci, A. Falcicchio, A. Moliterni, R, Rizzi, *J. Appl. Crystallogr.* 48 (2015), 598.

[33] A. Altomare, C. Cuocci, C. Giacovazzo, A. Moliterni, R. Rizzi, N. Corriero, A. Falcicchio, *J. Appl. Crystallogr.* 46 (2013), 1231.

[34] A. Gražulis, D. Chateigner, R. T. Downs, A. F. T. Yokochi, M. Quirós, L. Lutterotti, E. Manakova, J. Butkus, P. Moeck, A. Le Bail *J. Appl. Crystallogr.* 42 (2009), 726.

[35] D. Massiot, F. Fayon, M. Capron, I. King, S. Le Calvé, B. Alonso, J. O. Durand, B. Bujoli, Z. Gan, G. Hoatson, *Magn. Reson. Chem.* 40 (2002), 70.

[36] N. M. Dicaire, F. A. Perras, D. L. Bryce, *Can. J. Chem.* 92 (2014) 9.

[37] J. B. d'Espinose de Lacaillerie, C. Fretigny, D. Massiot, *J. Magn. Reson.*192 (2008**)**, 244.

[38] J.-P. Amoureux, C. Fernandez, S. Steuernagel, *J. Magn. Reson. Ser. A* 123 (1996), 116.

[39] B. Gee, H. Eckert, *Solid State Nucl. Magn. Reson* 5 (1995), 113.

[40] H. Eckert, Z. Phys. Chem. 224 (2010), 1591..

[41 D. Zhao, Z. Xie, J. M. Hu, H. Zhang, W. L. Zhang, S. L. Yang, W. D. Cheng, *J. Mol. Struct.* 922 (2009), 127.

[42] J. L. Rodrigo, P. Carrasco, J. Alamo, *Mater. Res. Bull.* 24 (1989), 611.

[43] T. Gullion, A. J. Vega, *Prog. Nucl. Magn. Reson. Spectrosc.* 47 (2005)123.

[44] R.D: Shannon, *Acta Crystallogr.* A 32 (1976), 751

[45] F. Behrends, H. Eckert, *J. Phys. Chem.* C 118 (2014), 10271.

[46] Y. Zhu, Y. Zhang, L. Lu, *J. Power Sources* 290 (2015), 123.